PROCEEDINGS, 46th Workshop on Geothermal Reservoir Engineering
Stanford University, Stanford, California, February 15-17, 2021
SGP-TR-218

Evolution of Fluid Transmissivity and Strength Recovery of Shear Fractures under Hydrothermal Conditions

Tamara Jeppson, David Lockner, Brian Kilgore, Nicholas Beeler and Joshua Taron

345 Middlefield Rd., MS977, Menlo Park, CA 94025

tjeppson@usgs.gov

Keywords: Transmissivity, shear fractures, strength, healing, sealing

ABSTRACT

Geothermal systems rely on the presence of long-lived and high-volume, permeable fracture systems. The creation, reactivation, and sustainability of these systems depend on complex coupling among thermal, hydraulic, mechanical, and chemical (THMC) processes occurring in geothermal reservoirs. In part due to a paucity of experimental data, the evolution of fractures at geothermal conditions in response to THMC processes is poorly understood, particularly during the process of shear. We present preliminary results of triaxial slide-hold-slide experiments, with hold periods ranging in duration from 103 s to 106 s, to constrain rates and mechanisms of healing and sealing. Experiments were conducted on simulated fault gouge composed of Westerly granite and on bare surfaces of Westerly granite. The tests were run at temperatures of 22˚ and 200˚ C with confining and average pore pressures of 30 MPa and 10 MPa, respectively. We used an axial displacement rate of 0.1 μm/s during sliding periods. Deionized water flowed continuously along the simulated fracture so we could determine in-plane fluid transmissivity during the tests. In gouge and bare surface experiments conducted at 200˚ C, we observe significant decreases in fluid transmissivity over the course of the experiments. For the hydrothermal gouge experiment we measured an order of magnitude net reduction in transmissivity from 1.73x10-18 to 0.17x10-18 m3, over the course of 220 hours while in the room temperature gouge experiment transmissivity only decreased by 0.35x10-18 m3 over the same amount of time. In the experiments, we observe an up to 16% recovery in fluid transmissivity during sliding periods. At room temperature the friction data showed limited fault re-strengthening with time; healing rates are on the order of 0.1 MPa/decade. A similar healing rate was observed at 200˚ C in the gouge but we observe an increase in the healing rate, to 0.75 MPa/decade, for a bare surface experiment at 200˚ C. The differences in the healing rate of the gouge and bare surface experiments suggest that the generation of fine particles by grinding down of asperities on the bare surface promote quartz dissolution and reprecipitation at elevated temperatures. Further work is needed to test this possibility and provide better constraints on factors influencing the evolution of fluid transport properties and strength of shear fractures at geothermal conditions.

1. INTRODUCTION

Economically viable geothermal reservoir operations rely on the presence of long-lived and large-volume permeable fracture systems with a high heat transfer area. The properties of these fracture systems evolve over time in response to complex interactions among thermal, mechanical, chemical, and hydraulic (THMC) processes. When these interactions result in a loss of permeability, hydraulic or thermal stimulation is used to create or reactive flow pathways. Although stimulation methods are generally effective at generating permeability within EGS reservoirs (*e.g.,* Chabora et al., 2012; Plummer et al., 2016), the magnitude of this response and its persistence over sustained periods of thermal and chemical disequilibrium remain poorly understood. This uncertainty is partially related to the fact that interactions between THMC processes within fractures are not well constrained. This paper describes an experimental investigation of the joint evolution of fluid transport properties and strength in simulated shear fractures.

There has been some investigation into the evolution of fluid transport properties of static fractures at geothermal conditions. These studies have been conducted on granite at temperatures ranging from 150˚ to 500˚ C (Moore et al., 1994; Morrow et al., 2001), ultramafic rocks at 260˚ C (Farough et al., 2016), and novaculite at temperatures up to 150˚ C (Polak et al., 2003; Yasuhara et al., 2006). These studies indicate that in fractured samples permeability decreases faster at a given temperature than in the intact counterparts. In some of these tests the fracture surface showed evidence of dissolution and mineral growth increasing with both time and temperature (Morrow et al., 2001; Farough et al., 2016.

Recently, greater attention has been given to examining how fluid transport properties evolve with shear stress and displacement at room temperature (*e.g.,* Faoro et al., 2009; Rutter & Mecklenburgh, 2017, 2018; Ye et al., 2017; Im et al., 2018, 2019). These studies show that permeability decreases significantly during initial sliding on the fracture surface due to the grinding down of asperities and generation of wear products, but subsequent reactivation of the surface after a hold period tends to result in permeability enhancement due to shear dilation. The permeability also gradually decreases with time in the intervals between shearing; longer-duration hold intervals may result in greater permeability enhancement upon reactivation (Im et al., 2018).

A time-dependent change in rheological properties is also observed in frictional studies. In slide-hold-slide (SHS) experiments intervals of shearing are separated by quasi-static hold periods. These tests provide a simple analog for the seismic cycle (induced or naturally occurring) with the slip and hold periods representing coseismic and interseismic periods. In theses tests, the static friction increases with the hold duration (Dieterich, 1972). This restrengthening behavior has been observed under a range of conditions in different materials (*e.g.,* Beeler et al., 1994; Carpenter et al., 2016a, 2016b; Karner & Marone, 2000; Tesei et al., 2012). Several recent studies have indicated

that the magnitude of restrengthening depends on the magnitude of shear stress during the hold period and that at low shear stress the shear fracture may exhibit time-dependent weakening instead of strengthening (Nakatani, 1998; Karner & Marone, 2001; Ryan et al., 2018). However, most of these studies were conducted under room temperature and nominally dry conditions that are not relevant to geothermal reservoirs.

A few studies have examined restrengthening behavior at geothermal conditions. In some of these studies the hold and slide periods were conducted under very different temperature (hold: 450˚ to 927˚ C; slide: room temperature to 230˚ C), confining pressure (holds: 250 MPa; slide: 50 to 250 MPa), and saturation conditions (hold: saturated; slide: nominally dry or saturated) making these studies less relevant to geothermal reservoirs (Karner et al., 1997; Tenthorey et al., 2003). Nakatani & Scholz (2004) examined strength recovery in saturated quartz gouges at temperatures from 100˚ to 200˚ C and Lockner et al. (2019) performed similar experiments on bare surface Eureka quartzite. In both of these studies the rate of restrengthening increased with temperature, hypothesized to be due to a solution transfer mechanism. Limited data acquired for holds at reduced shear stresses suggests that under geothermal conditions strength recovery is independent of shear stress during the hold (Nakatani & Scholz, 2004).

In frictional studies the term healing is often used interchangeably with strength recovery, or restrengthening. Healing indicates the loss of memory of the pre-healed, or damaged, state of a material through a variety of processes including mineral transformations, pressure solution, dissolution/precipitation, gouge densification/cementation, and sealing. However, sometimes healing refers to chemical processes which, especially at room temperature, may not be related to strength recovery. For the purposes of this paper, we will use healing and restrengthening interchangeably to refer to the difference between steady-state sliding friction and the static friction measured upon the resumption of sliding following a hold period in a slide-hold-slide experiment.

Studies examining the joint evolution of fluid transport properties and strength with time and slip are rare in the literature. In tests on bare surface granite at room temperature no significant changes in the fluid transport or frictional properties were observed for holds lasting up to 20 days (Kishida et al., 2011). Olsen et al. (1998) examined restrengthening and sealing, defined as the overall permeability reduction, under geothermal conditions in simulated gouge composed of quartz and labradorite. Some recovery of permeability was observed during sliding but there was an overall loss of permeability over the course of the experiment thought to be caused by secondary mineral precipitation. Olsen et al. (1998) did not observe clear static friction peaks upon reactivation of the fracture surface.

In order to elucidate how THMC processes affect fractures in geothermal reservoirs, we have carried out preliminary SHS experiments on simulated fractures, gouge-filled and bare surface, in Westerly granite under saturated conditions at an effective confining pressure of 20 MPa and temperatures of 22˚ and 200˚ C. This experimental work examines the evolution of fluid transport properties and strength as a function of time, temperature, and shear stress.

2. METHODOLOGY

2.1 Sample preparation

Frictional sliding experiments were performed in the conventional triaxial configuration. Forcing blocks (2.54 cm diameter x ~ 6.1 cm long) containing saw cuts inclined at 30˚ to the vertical axis were made from cylindrical samples of Westerly granite. Small (2.38 mm diameter) offset boreholes were drilled through the blocks to provide fluid access to the surface (Figure 1). The sawcut surfaces were ground flat and then scribed with a 6 to 7 mm long groove intersecting the borehole perpendicular to the long axis of the sawcut surface. These grooves were added to facilitate near-parallel flow between boreholes in the bare surface tests. The grooves are shallow and likely have no effect on flow in the gouge tests. The surface was then roughened using #240 silica carbide abrasive powder, producing an root-mean-square (RMS) roughness of 5 μm. At this point, bare surface samples were assembled and placed in a lead tube with 1.0 mm wall thickness. For gouge samples, small stainless-steel inserts (1.0 mm ID and 2.1 mm OD) were placed in the boreholes which were then backfilled with quartz sand (~ 500 μm diameter) to prevent loss of gouge particles while maintaining flow of the pore fluid. A simulated gouge was prepared from crushed Westerly granite with particle size less than 90 μm. The powder was mixed with deionized water to form a paste that was spread in a 1 mm thick layer on the sawcut surface of one forcing block before being sandwiched by a second block and inserted into the lead jacket. Double viton O-rings on both ends of the jacket provided seals to isolate the sample and pore fluid from argon gas used to apply confining pressure.

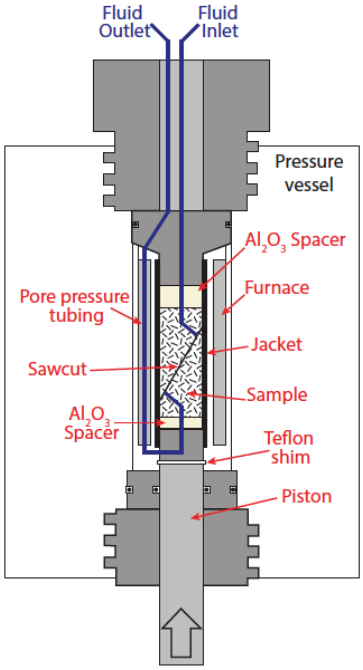

Figure 1: Schematic of the triaxial apparatus and sample geometry used in this study. An internal thermocouple was placed in the fluid inlet to monitor temperature and provide feedback for the furnace. A greased teflon shim accommodated later slip between the sample assembly and loading piston.

2.2 Experimental procedure

The sample assembly was inserted into a furnace and placed in the pressure vessel as illustrated in Figure 1. A greased Teflon shim was placed between the sample assembly and the forcing piston to accommodate lateral slip of the lower forcing block during shear. The sample and pore pressure system were evacuated before increasing confining pressure to approximately 15 MPa using argon gas as the confining medium. At that point, pore fluid (deionized water) was introduced to the evacuated sample and pore pressure was raised to 10 MPa. Confining pressure was then raised to the target value of 30 MPa and the temperature was increased to 200°C over a period of 40 to 60 minutes. Calibration tests on dummy samples were conducted to determine the furnace temperature profile. The sample assemblies incorporated alumina spacers to position the sawcut in the center of the furnace so that temperatures reported here refer to the maximum temperature at the center of the sawcut. Temperature at the ends of the sawcut are 3.4% lower. Boreholes drilled through the alumina spacers and granite blocks allowed access for the pore fluid and the thermocouple used to control temperature. The thermocouple was placed in the borehole at the top of the upper driving block and generally maintained temperature to within ± 0.5°C with occasional fluctuations of up to ± 2°C. Unless otherwise noted experiments were run under conditions of constant confining pressure. However, in one experiment, normal stress was held constant at 45 MPa (35 MPa effective) by changing confining pressure under computer control.

Previous work has shown that the fault surface or gouge layer alters rapidly upon initiation of sliding (e.g., Lockner et al., 1986; Logan & Rauenzahn, 1987; Biegel et al., 1989; Marone & Scholz, 1989) so we began each experiment with an initial 0.9 mm axial displacement run-in at a rate of 1 μm/s followed by 0.1 mm of displacement at 0.1 μm/s to achieve steady state sliding. Axial displacement was then halted, beginning the first hold period. Each hold has a specified duration (t_h) followed by 0.25 to 0.30 mm axial displacement at a rate of 0.1 μm/s. Axial displacement (measured on the piston outside of the pressure vessel) was corrected for the elastic deformation of the loading system and inclined fault geometry to calculate the slip resolved on the sawcut, assuming all permanent sample shortening was due to slip. Real time corrections for seal friction and changes in cross-sectional area due to slip (Scott et al., 1994; Tembe et al., 2010) were applied when calculating the stress during the experiment. We applied a correction for jacket strength; as lead has a low strength, high ductility, and essentially no strain hardening, these corrections are small (approximately 0.34 MPa shear stress at 200°C and 0.94 MPa at 22°C) (Moore & Lockner, 2011). Most importantly for these experiments, the lead jackets deform plastically, so shear stress peaks observed upon re-initiation of slip are not jacket artifacts.

In conventional SHS experiments, when loading is stopped the axial piston remains in position and shear stress gradually relaxes during the hold via creep at the slip surface. Some previous studies have sought to reduce the amount of creep by retracting the piston to reduce the shear stress during the hold. We similarly examine the effect of shear stress during the hold period by conducting both conventional, or high shear stress holds, and unloaded holds with different levels of reduced shear stress. For these reduced shear stress holds, when the slide period is completed, the piston is retracted at a rate of 10 μm/s for a specified distance after which the load-point velocity is set to zero. At the end of the hold period the axial piston is advanced at a rate of 1 μm/s until the piston is 0.02 mm away from the final position reached prior to unloading. The reloading rate is then decreased to 0.1 μm/s so that the sample is loaded at the same rate as in preceding slide periods. The time required to bring the piston back to its starting position can be a significant fraction of the hold period, especially for holds of short duration. Therefore, we define the hold duration to include both the stationary hold period (where load-point velocity is

zero) and the time required for the piston to return to its pre-hold position. Following Karner & Marone (2001), we quantify the shear stress during the hold as:

$$\eta = \frac{\tau_{hold}}{\tau_{ss}} \tag{1}$$

where τ_{hold} is the shear stress at the start of the hold period and τ_{ss} is the steady state shear stress during the preceding slide. This definition leads to η=1 for conventional SHS and η=0 if the sample if completely unloaded during the hold period.

2.2.1 Defining steady-state for unstable slides

Restrengthening, $\Delta\mu$, is the difference between friction at peak static friction (μ_{peak}) and steady state sliding friction (μ_{ss}) measured in a slide-hold-slide experiment (Figure 2a). Nakatani & Scholz (2004) proposed the following model for restrengthening as a function of time:

$$\Delta\mu = b\ ln\left(\frac{t_h}{t_c} + 1\right) \tag{2}$$

where b is the log-linear restrengthening rate and t_c is a characteristic time delay before the onset of strengthening. In a standard sequence of SHS tests, peak strength is followed by a return to steady-state friction and eq. (2) can be used to determine b and t_c. However, in many of our high temperature SHS sequences, peak stress was followed by relatively rapid weak stress drops as indicated in Figure 2b. As the definition of restrengthening requires the identification of a steady state friction value, this behavior is problematic. In this case, we assert that the small-amplitude stress drops also satisfy eq. (2) with t_h given by the inter-event times. Then, we jointly fit the main peak stress and subsequent small event peaks, solving for b, t_c and $\Delta\mu_0$ in

$$\mu_{peak} = b\ ln\left(\frac{t_h}{t_c} + 1\right) - \Delta\mu_0, \tag{3}$$

where $\Delta\mu_{peak} = (\mu_{peak} - \mu_0)$ and $\Delta\mu_0 = (\mu_0 - \mu_{ss})$ with μ_0 defined as a reference value, which, for convenience, we choose to be approximately equivalent to the peak friction of the small events. Substitution of these definitions into eq. (3) shows that it is equivalent to eq. (2) and provides a method for estimating the model parameters in the absence of steady sliding. Cutoff time is typically t_c > 1000s while the small, rapid events are separated by ~10 to 100s. As the Nakatani and Scholz (2004) model predicts little to no restrengthening with time for hold durations less than the cutoff time which they determined to be 1193s at 200C, these small slip events provide a constraint on μ_{ss} and the main SHS events constrain b and t_c.

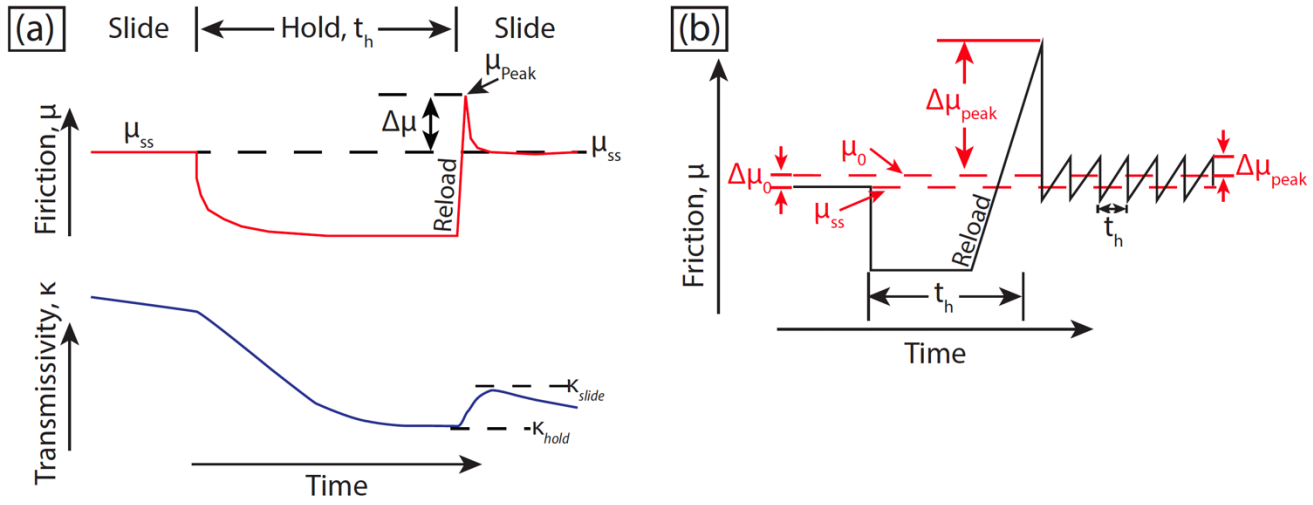

Figure 2: Schematic diagrams of restrengthening and transmissivity with time during slide-hold-slide experiments (a) Evolution of restrengthening and transmissivity during hold and sliding periods. Restrengthening, given by Δμ, is defined as the difference between static friction (μ_{peak}) and steady-state sliding friction (μ_{ss}). Recovery of transmissivity is defined as the log of the ratio of the maximum transmissivity during sliding (κ_{slide}) and the transmissivity at the end of the preceding hold period (κ_{hold}). (b) Schematic of restrengthening when slip is unstable, showing definitions of variables used to solve for steady-state friction.

2.2.2 Transmissivity

Mean pore pressure in all samples was 10 MPa. To measure transmissivity, a pore pressure differential was imposed between the two boreholes in the sample to produce a steady-state flow regime. In most tests, this differential was 2 MPa (9 and 11 MPa at the two boreholes). However, at the beginning of the gouge experiments the permeability was too high for the pore pressure pump to produce this gradient. In this case the differential was reduced to 0.5 MPa. The flow-through experiments were conducted in two configurations: 1)

semi-continuous flow in one direction or 2) cyclic flow reversals. In the semi-continuous flow experiments the upper borehole was maintained as the high side of the pressure differential and fresh deionized water was continuously supplied to the sawcut except when one of the pore pressure pumps reached the end of its stroke and needed to be refilled or emptied. During these refill periods the pump was isolated from the sample. For the cyclic flow tests the pressure differential was imposed producing a steady-state flow regime. After a set volume of fluid (~ 2 ml) was passed through the sample, flow direction was reversed so the same volume of fluid was flowed back and forth through the sample. For long hold periods, after most of the fluid volume had passed through the sample the pressure differential was removed and pore pressure was held constant at 10 MPa for a period of time before reversing the flow direction.

For intact samples, flow-through tests are typically used to determine permeability using Darcy's law or some equivalent. For a fracture dominated system, measured flow rate is also affected by aperture which we do not measure directly. Thus, we report a variation of the fracture's hydraulic transmissivity which we define as the product of the permeability (k) and fracture aperture (a). Transmissivity defined this way is commonly used to describe the fluid transport properties of a fracture when aperture is unknown (Zimmerman & Bodvarsson, 1996; Rutter & Mecklenburgh, 2017, 2018;). However, it is not the usual definition of hydraulic transmissivity, which is typically reported as the product of the hydraulic conductivity (K) and aperture. The two definitions of transmissivity are related as shown:

$$\kappa = \frac{\kappa_K \nu_f}{\rho g} = \frac{\nu_f Q L}{w \Delta P} \tag{3}$$

where κ is the transmissivity calculated from permeability, κ_K is the transmissivity calculated from hydraulic conductivity, ν_f is the dynamic viscosity of water (0.136 cP at 200°C), ρ is the fluid density, g is gravitational acceleration, Q is the volumetric flow rate, L is the distance between the boreholes, w is the length of the groove cut into the sawcut surface, and ΔP is the pore pressure differential. Flow rate through the sample is based on flow rate measured at the pore pressure pump at room temperature so assuming conservation of fluid mass the flow rate at elevated temperature is calculated as:

$$Q_{200℃} = Q_{22℃}\left({V_{200℃}}/{V_{22℃}}\right) \tag{4}$$

Where V is the specific volume of water ($V_{200°C}$ = 0.0011 m^3/kg at 20 MPa) and the subscript denotes the temperature in degrees Celsius. Typical errors in the transmissivity values are ±3.5% and the lower limit for transmissivity measurement is $1x10^{-22}$ m^3. We calculated transmissivity for 15-minute intervals of flow. This time interval provides enough data to constrain the flow rate while being small enough to fit within the shortest hold period.

3. RESULTS

3.1 Low shear stress holds at room temperature

An initial set of experiments was conducted at room temperature. Each hold duration was repeated up to three times in succession at different shear stresses. The samples exhibit strain hardening behavior with the steady state friction values ranging between 0.65 and 0.74 for the Westerly granite gouge and between 0.63 and 0.74 for Westerly granite bare surface, consistent with previous studies under similar conditions (Kilgore et al., 1993; Ryan et al., 2018).

Figure 3 shows restrengthening with η observed in this study and previous work by Ryan et al. (2018). The data from this study, circles and triangles on Figure 3, shows that the magnitude of restrengthening increases with η for both the Westerly granite gouge and bare surface experiments (Figure 3). This is observed at all the hold durations examined in this study. Both the gouge and bare surface tests show, on average, a 0.008 decrease in $\Delta\mu$ for a 0.62 decrease in η at constant confining pressure. This trend is opposite of that observed in previous SHS experiments (x's and +'s on Figure 3), which used a biaxial configuration, where it was found that $\Delta\mu$ increased with decreasing η for gouges and no clear trend for bare surface samples was observed (Nakatani & Mochizuki, 1996; Nakatani, 1998; Karner & Marone, 2001; Ryan et al., 2018). Direct comparison of the magnitude of restrengthening observed by Ryan et al. (2018) to the results of this study shows that the restrengthening in gouge experiments measured at η=1 is consistent but the triaxial bare surface tests tend to display less restrengthening than was observed in the biaxial configuration.

For better comparison with previous biaxial experiments, we also conducted a gouge experiment at a constant normal stress of 35 MPa, consistent with the steady-state normal stress during the constant confining pressure tests. At constant normal stress we do not observe a clear relationship between restrengthening and shear stress. The magnitude of restrengthening decreases as η increases from 0.16 to 0.34 but there is little to no change in $\Delta\mu$ for η > 0.34. Although there is variability, results of the normal stress experiment are generally consistent with restrengthening measured at η=1 in the constant confining pressure tests.

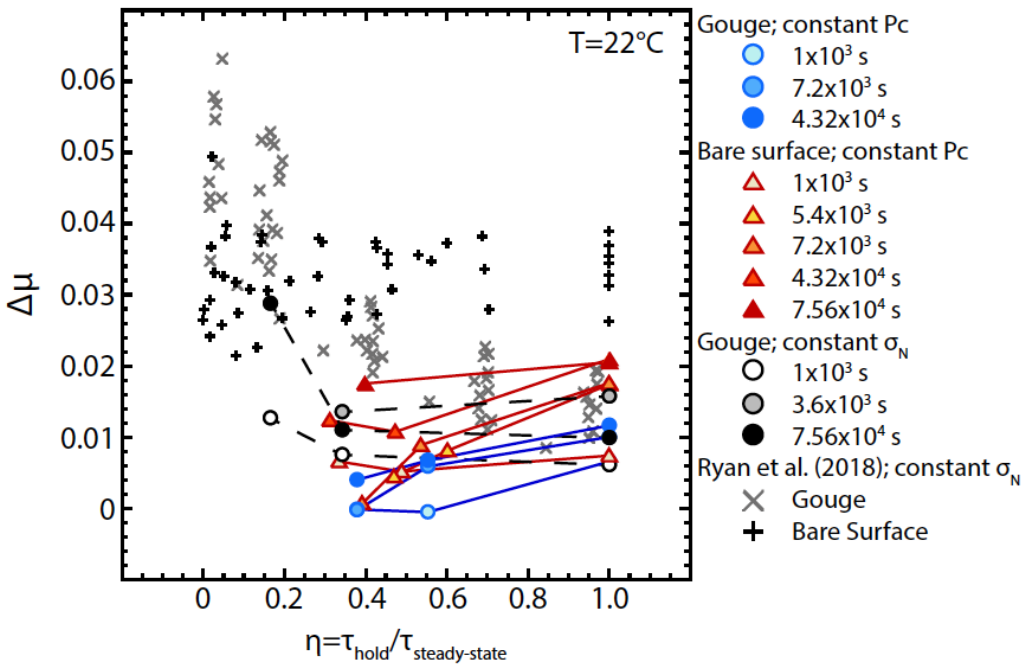

Figure 3: Restrengthening versus normalized shear stress during hold period (η) for Westerly granite gouge (blue circles) and bare surface (red triangles) experiments at 22 ˚ C under constant confining pressure (Pc). Restrengthening for Westerly granite gouge experiments under constant normal stress (σ_N; black circles) are also shown alongside data from Ryan et al. (2018)'s Westerly granite bare surface and gouge experiments. Our data show a decrease in strengthening with decreasing η in contrast to trends observed by Ryan et al. (2018).

3.2 Restrengthening at hydrothermal conditions

For experiments conducted at 200˚ C we observe an increase in the steady-state friction which ranges between 0.70 and 0.78 for the Westerly granite gouge and between 0.67 and 0.86 for the Westerly granite bare surface. A slight increase in steady-state friction with the increase in temperature to 200 ˚ C is in agreement with previous studies (Blanpied et al., 1991, 1995; Mitchell et al., 2013) but a 0.86 coefficient of friction for the bare surface is higher than anticipated. Similar to room temperature tests, experiments run at 200˚ C also show less restrengthening for holds at low shear stress. For the gouges, $\Delta\mu$ ranges between 0.0006 and 0.01 when η=1 and between -0.009 and 0.002 for η < 1 (Figure 4a). The bare surface experiments show an even greater contrast with $\Delta\mu$ ranging between 0.02 to 0.05 when η =1 and between 0.008 and .02 for η <1 (Figure 4b).

For η=1, the average healing rate for the gouges is 0.23 MPa/decade at room temperature and 0.11 MPa/decade at 200˚ C (excluding the anomalously high value recorded for t_h=10^3 s). In contrast, at room temperature the average bare surface healing rate is 0.39 MPa/decade while the healing rate at 200˚ C is 0.75 MPa/decade. No clear time dependence is observed for results acquired at η <1. The healing rate of the bare surface samples at η=1 is comparable to the healing rate observed in previous studies at 200˚ C on quartz gouge (Figure 5; Nakatani & Scholz, 2004) and bare surface quartzite (Lockner et al., 2019).

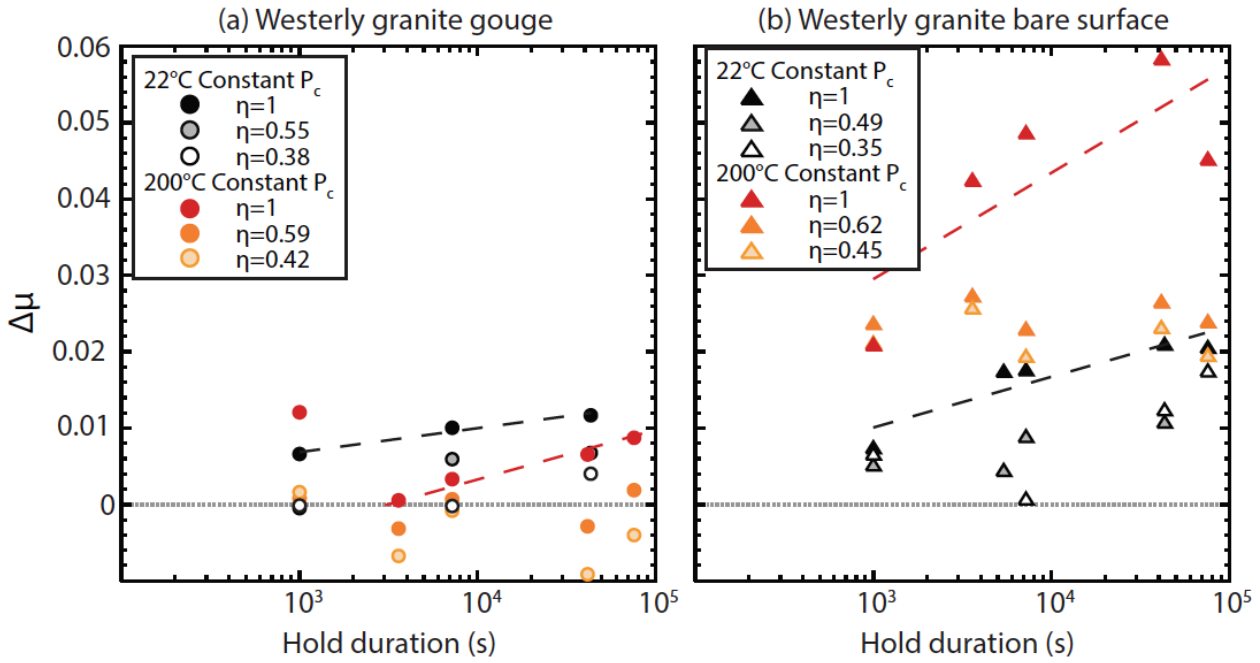

Figure 4: Restrengthening versus hold duration at 22° and 200°C for Westerly granite (a) gouge and (b) bare surface experiments. For room temperature experiments samples exhibit limited restrengthening with time. The slow healing rate persists in the gouge at higher temperature but for bare surface a significant increase in healing rate is observed at 200°C when the normalized shear stress (η) is equal to one. Gray scale symbols represent measurements made at 22°C while red and orange represent measurements made at 200°C. The gradation in color indicates decreasing η, with red and black representing η=1.

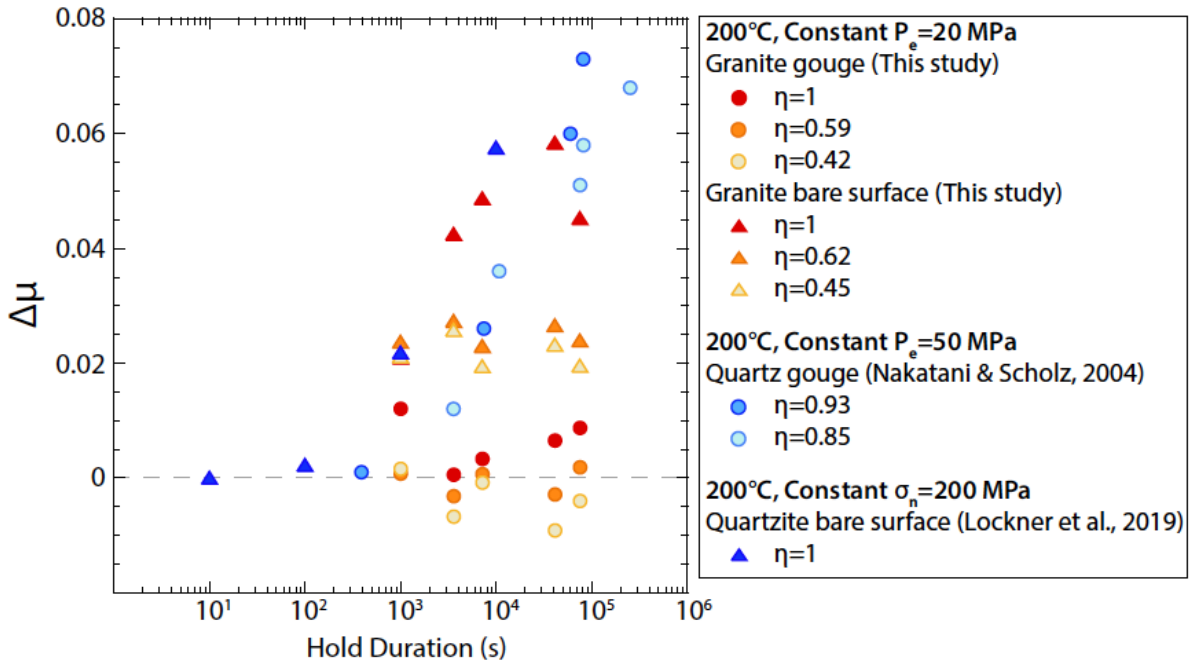

Figure 5: Comparison of restrengthening versus hold duration for Westerly granite (red) and quartz (blue). Circles indicate date from gouge experiments while triangles are for bare surface data. Dark blue and red indicates data from hold where η=1 with lighter shades indicating decreasing η. Bare surface granite at η=1 and quartz samples exhibit a faster healing rate than the granite gouge and low η bare surface data.

3.3 Transmissivity

In Figure 6 we examine the evolution of transmissivity with time at 22˚ C and 200˚ C, starting at the beginning of the first hold. Over the course of a 220-hour experiment at room temperature the transmissivity of the gouge decreases by 0.35×10^{-18} m^3 (Figure 6a). In experiment conducted at 200 ˚ C the transmissivity decreases by 1.6×10^{-18} m^3 over the same amount of time (Figure 6b). Similarly, for bare surface, the transmissivity decreases by 0.035×10^{-19} m^3 at room temperature and 4.6×10^{-19} m^3 at 200˚ C over the course of a 50-hour test (Figure 6c & d). The hydrothermal experiments undergo a significantly greater reduction in transmissivity, but their initial transmissivity is also higher than for their low temperature counterparts. The initial gouge transmissivity at 22˚ C and 200˚ C is 5.8×10^{-19} m^3 and 18×10^{-19} m^3, respectively, for gouge and 0.23×10^{-19} m^3 and 5.7×10^{-19} m^3, respectively, for bare surface. This difference in transmissivity could be a thermo-mechanical effect or it could reflect variability in the samples.

Transmissivity increases during some of the sliding periods. In the gouge experiments, the transmissivity increases by 1.4×10^{-19} m^3 at 22˚ C and by 0.32×10^{-19} m^3 at 200˚ C during the slide following a 5×10^5 s hold (Figure 6a & b). We define transmissivity recovery (R) as:

$$R = \log\left(\frac{\kappa_{slide}}{\kappa_{hold}}\right), \tag{5}$$

where κ_{slide} is the maximum transmissivity during the slide and κ_{hold} is the transmissivity at the end of the preceding hold. This definition yields R=0 when there is no change in transmissivity and provides equal weight to increases and decreases in transmissivity. The recovery in transmissivity during sliding is plotted against both hold duration and restrengthening in Figure 7. Despite some scatter, there are identifiable trends in the bare surface data. For bare surface experiments at all values of η, there tends to be an increase in transmissivity recovery with hold duration, but a positive correlation between recovery and restrengthening is only seen when η=1. The highest healing rate was also observed for bare surface tests when η=1. A linear fit to these data gives $dR/d\Delta\mu \approx 8$.

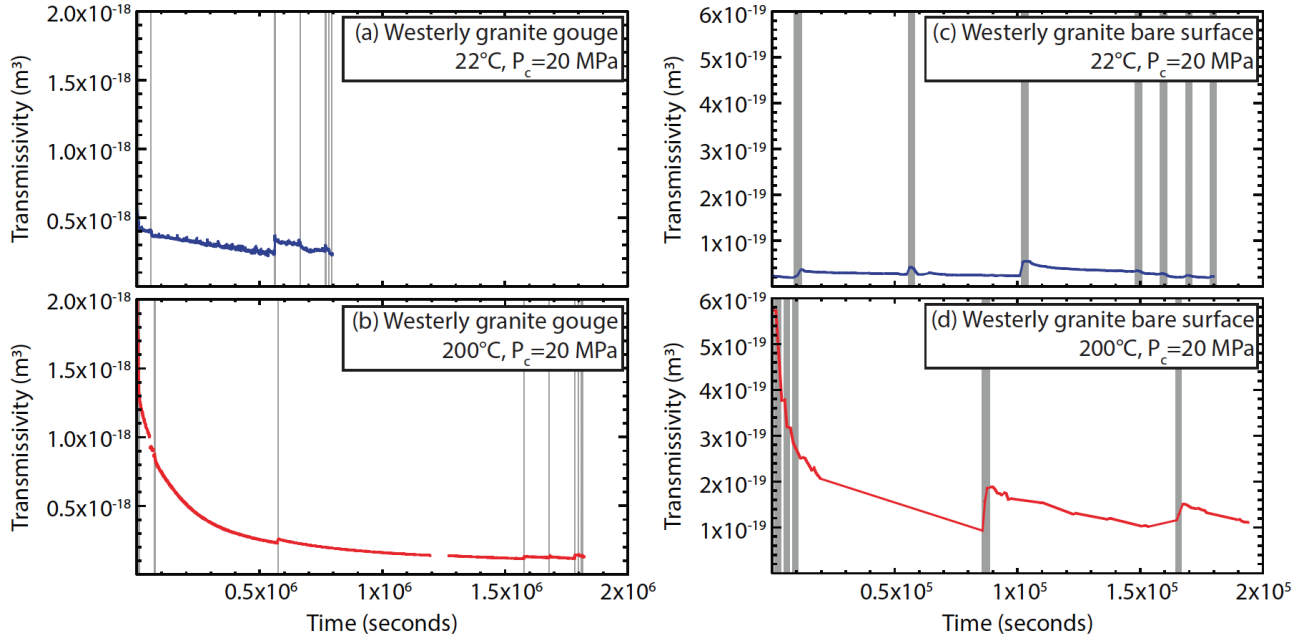

Figure 6: Change in transmissivity with time at 22° and 200°C for Westerly granite gouge (a & b) and bare surface (c & d) experiments. Data are shown from the beginning of the first hold to the end of the experiment. Vertical gray bars indicate times when the sample was undergoing shear displacement. An order of magnitude greater reduction is observed at 200°C than at room temperature. Some sliding periods are associated with increases in transmissivity.

4. DISCUSSION

4.1 Effect of shear stress

Our data show that, under conditions of constant confining pressure, restrengthening is reduced for both granular fault gouge and bare rock surfaces during holds at low shear stress. Additionally, restrengthening during these low shear stress holds shows little to no time-dependence. Our results are opposite of those reported in previous studies, which reported time-dependent weakening for $\eta < 0.9$ and found that the magnitude of restrengthening decreased with increasing η in gouge experiments while restrengthening was observed to be independent of η in bare surface experiments (Nakatani, 1998; Nakatani & Mochizuki, 1996; Karner & Marone, 2001; Ryan et al., 2018). These earlier experiments were focused on probing rate & state friction laws, so experiments were conducted under nominally dry conditions at room temperature and short time scales in a double direct shear configuration in a biaxial testing apparatus.

A simple explanation for the difference in the results could lie in the definition of hold duration. Previous studies defined hold duration as the time from when the reduced shear load was reached to the time that reloading began, while we included the reloading time in the

hold duration. The more the shear load is reduced the more time is required to reload the sample before the surface will begin to slide again. At short time scales this can significantly increase the duration of the quasi-stationary hold period between sliding periods. Thus, if restrengthening is time dependent, holds conducted at lower shear stresses would appear to undergo more restrengthening than holds at higher shear stress. Ryan et al. (2018) reloaded at a rate of 10 μm/s, when η =0.02 this adds additional 50 s to the reload time. Assuming that the decrease in restrengthening observed by Ryan et al. (2018) at higher η is due to the increased reloading time, we can calculate the expected increase in $\Delta\mu$ due to this additional reloading time. Using a healing rate of 0.37 MPa/decade measured at room temperature on granite gouge with η=0.97 (Nakatani, 1998) we would expect a 0.003 increase in $\Delta\mu$. This change in not enough to explain the trend observed by Ryan et al (2018) or the difference between our data and that of Ryan et al. (2018).

It is more likely that the difference between our results and those of previous studies is due to a difference in experimental conditions. It has been hypothesized that the increased restrengthening of gouge at low η, when under constant normal stress, occurs because the decrease in shear stress facilitates particle rearrangement and compaction, assisted by the normal stress, leading to an increase in gouge density and greater strength. In contrast, for constant confining pressure triaxial tests, reduction in shear stress is accompanied by reduction in normal stress on the inclined fault. The reduction in normal stress would lead to less compaction and thus less restrengthening during the hold period. However, in our constant normal stress test on a gouge sample the magnitude of restrengthening showed no dependence on shear stress for η > 0.4 and is generally consistent with restrengthening measured for η=1 when tested at constant confining pressure. However, the constant normal stress data do show an increase in restrengthening for η<0.4. More work needs to be done to determine if constant normal stress conditions can explain the differences in observed restrengthening. Additional factors to explore in future work include transient fluid pressure effects and the potential for damage of grain contacts due to reworking of gouge during the reloading phase of the low shear stress holds.

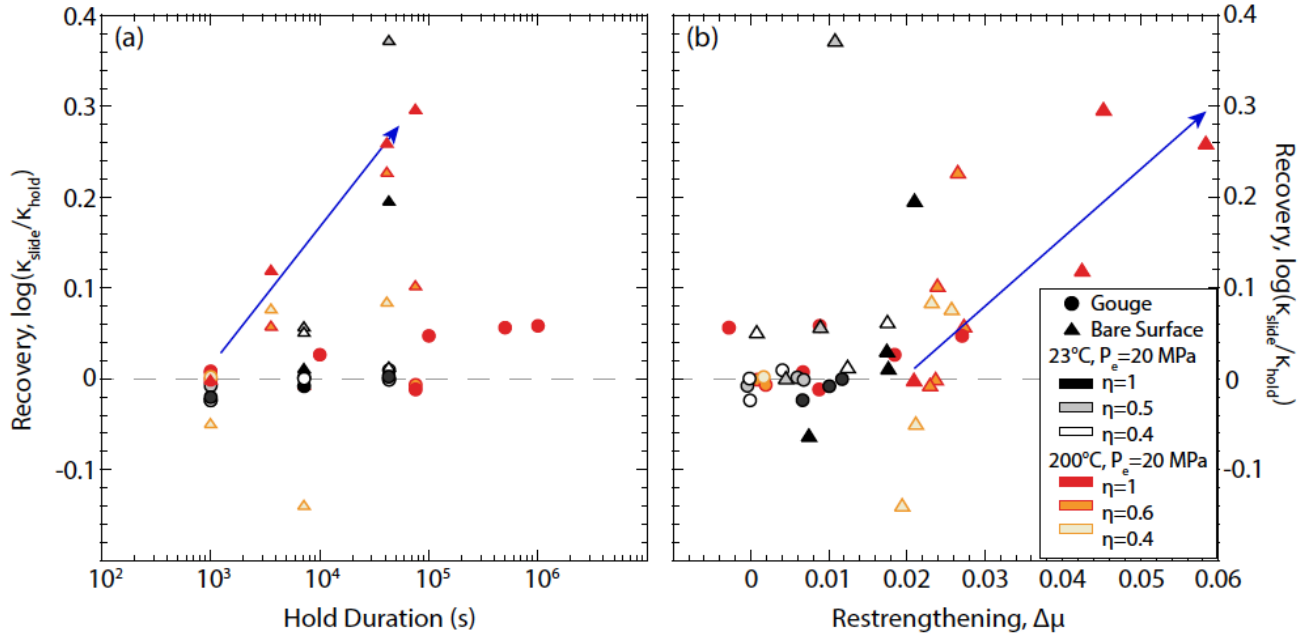

Figure 7: Recovery of transmissivity versus (a) hold duration and (b) restrengthening. Bare surface data (triangles) at measured at 200°C and η=1 (red) show a positive correlation between recovery and hold duration or restrengthening (indicated by blue arrows). Data acquired at lower η usually have similar magnitudes of transmissivity recovery at the same hold times but lower magnitudes of restrengthening.

4.2 Temperature and healing rate

At hydrothermal conditions we do not observe restrengthening for holds at low shear stress. However, for conventional SHS tests (η=1), the healing rate for the bare surface samples is much higher at hydrothermal conditions than at room temperature but there appears to be no temperature dependence for the gouges.

The majority of work examining frictional restrengthening has been done at room temperature with only a few studies examining the behavior at hydrothermal conditions. The experiments presented in this study are most directly comparable to previous work by Lockner et al. (2019), Nakatani & Scholz (2004), and Olsen et al., (1998). In those studies, SHS experiments were conducted under constant confining pressure (Olsen et al., 1998; Nakatani & Scholz, 2004) or constant normal stress (Lockner et al., 2019) in a conventional triaxial configuration under hydrothermal conditions at temperatures up to 250˚ C. Olsen et al. (1998) used simulated gouge composed of a mixture of quartz and labradorite while Nakatani & Scholz (2004) and Lockner et al. (2019) used quartz powder and bare surface quartzite, respectively. Olsen et al. (1998) conducted their experiments with shear stress during hold period decreased to η ~ 0.93. They defined healing as the difference between the steady-state sliding friction before and after the hold, so their estimates of healing cannot be directly compared to the values presented in this paper. Nevertheless, the absence of observable peak fiction upon reloading is consistent with the

lack of healing we observed for gouges in this study (Figure 5). Nakatani & Scholz (2004) also decreased the shear stress during the hold period. Most of their gouge experiments were conducted at $\eta \sim 0.85$ but limited comparison to data collected at $\eta \sim 0.93$ indicated there was no dependence on shear stress. We may see a greater effect of shear stress because we examined a greater range in η.

The healing rates for the bare surface Westerly granite (this study), quartz gouge (Nakatani & Scholz, 2004), and bare surface quartzite (Lockner et al., 2019) are all consistent (Figure 6) and significantly greater than for Westerly granite gouge samples. Healing rate depends on the accessibility of reactive minerals in the sample (Peters, 2009). The very fine particles generated by the wear and grinding of asperities on the bare surface have a higher surface area per unit volume than the larger particles that compose the simulated granite gouge. This higher surface area likely increases the accessibility of quartz promoting dissolution, facilitating creep and leading to a higher healing rate. While shearing in the gouge layer will also generate fine particles, the layer is thicker and thus may accomadate shearing in palces that did not heal during the hold. More analysis needs to be done to verify the validity of this hypothesis. An alternate hypothesis is that the healing rate in the gouges is influenced by the confining pressure and Nakatani & Scholz (2004) gouge experiments have a higher healing rate than the gouges in this study because they were conducted at a higher confining pressure.

The similarity between healing rates at 22˚ C and 200˚ C for Westerly granite suggests that the hold durations examined have not exceeded the cutoff time for Westerly granite gouge at 200˚ C. As cutoff time decreases with increasing temperature (Nakatani & Scholz, 2004), future tests on the gouge at a higher temperature or longer hold durations may yield a healing rate similar to that of the bare surface granite and the quartz experiments.

4.3 Recovery of transmissivity and healing

We observe a more rapid decrease in transmissivity with time at 200˚ C than at 22˚ C, especially early in the experiments. The reason for this early rapid reduction is not yet clear. If real, it could be due to continued evolution of the surface and gouge layer but we would expect to see a similarly large reduction the room temperature tests. As this is not observed, it suggests that it is a related to a thermally activated process not just a mechanical one. For the bare surface tests the high rate of transmissivity reduction is associated with an increase in the healing rate at 200˚ C suggesting the mechanisms behind these changes are both reducing the fracture aperture and increasing contact area. In the gouge experiments, the reduction in transmissivity without associated increase in healing rate at 200˚ C suggests that the pore throats are being reduced without significant change to the contact area.

We also observe a positive correlation between the magnitude of recovery of transmissivity during sliding and hold time that is especially evident for high temperature bare surface experiments. Comparing recovery and restrengthening shows a positive correlation for the bare surface data but only when η=1. This suggests that healing may be occurring during the holds at low shear stress, but that the process is reversed during the extended reloading.

5. CONCLUSION

Experiments on the evolution of transmissivity and strength in gouge-filled and bare surface fractures in Westerly granite at hydrothermal conditions have revealed that temperature has a greater effect on the healing rate of bare rock surfaces fractures than that of gouge-filled fractures. This may be due the griding down of asperities on the bare surface which generates ultra-fine particles, increasing surface area and promoting quartz dissolution. While high temperature only leads to increased restrengthening in the bare surface tests, high temperature also leads to more rapid transmissivity reduction in both gouge and bare surface experiments. This suggests that mechanisms behind the reduction in transmissivity in gouge are impacting the pore throats without significantly altering the contact area and associated strength recovery. We do observe a positive correlation between the magnitude of restrengthening during a hold and the recovery of transmissivity during the following slide, which is especially evident in high-temperature, bare-surface tests at η=1. The effect of shear stress during the hold is not yet clear. The lack of restrengthening observed in our current data could be due to an associated decrease in normal stress during the hold or to new damage incurred during the reloading period. We also cannot currently explain the differences in the relationship between restrengthening and η observed for experiments conducted in the triaxial versus biaxial configurations. Additional experiments are needed to examine the effects of normal stress and saturation as well as the potential for loss of healing during reloading. This work marks only the beginning of a longer-term project to identify the mechanisms behind the restrengthening and sealing observed in these experiments and to define the effects of various stress and temperature conditions.

REFERENCES

Beeler, N. M., Tullis, T. E., & Weeks, J. D.: The roles of time and displacement in the evolution effect in rock friction, *Geophysical Research Letters*, **21***,* (1994), 1987–1990.

Biegel, R. L., Sammis, C. G., & Dieterich, J. H.: The frictional properties of a simulated gouge having a fractal particle distribution. *Journal of Structural Geology*, **11**, (1989), 827–846.

Blanpied, M. L., Lockner, D. A., & Byerlee, J. D.: Fault stability inferred from granite sliding experiments at hydrothermal conditions. *Geophysical Research Letters*, **18** (1991), 609–612.

Blanpied, M. L., Lockner, D. A., & Byerlee, J. D.: Frictional slip of granite at hydrothermal conditions. *Journal of Geophysical Research: Solid Earth*, **100**, (1995), 13045–13064.

Carpenter, B. M., Ikari, M. J., & Marone, C.: Laboratory observations of time-dependent frictional strengthening and stress relaxation in natural and synthetic fault gouges. *Journal of Geophysical Research: Solid Earth*, **121**, (2016a), 1183–1201.

Carpenter, B. M., Collettini, C., Viti, C., & Cavallo, A.: The influence of normal stress and sliding velocity on the frictional behaviour of calcite at room temperature: Insights from laboratory experiments and microstructural observations, *Geophysical Journal International*, **205,** (2016b), 548–561.

Chabora, E., Zemach, E., Spielman, P., Drakos, P., Hickman, S., Lutz, S., Boyle, K., Falconer, A., Robertson-Tait, A., Davatzes, N., Rose, P., Majer, E., & Jarpe, S.: Hydraulic stimulation of well 27-15, Desert Peak geothermal field, Nevada, USA, *Proceeding,* 37th Workshop on Geothermal Reservoir Engineering, Stanford University, Stanford, CA (2012).

Dieterich, J. H.: Time-dependent friction in rocks, *Journal of Geophysical Research*, **77**, (1972), 3690–3697.

Faoro, I., Niemeijer, A., Marone, C., & Elsworth, D.: Influence of shear and deviatoric stress on the evolution of permeability in fractured rock, *Journal of Geophysical Research: Solid Earth*, **114,** (2009).

Farough, A., Moore, D. E., Lockner, D. A., & Lowell, R. P.: Evolution of fracture permeability of ultramafic rocks undergoing serpentinization at hydrothermal conditions: An experimental study, *Geochemistry, Geophysics, Geosystems*, **17,** (2016), 44–55.

Im, K., Elsworth, D., & Fang, Y.: The influence of Preslip Sealing on the Permeability Evolution of Fractures and Faults. *Geophysical Research Letters*, **45**, (2018).

Im, K., Elsworth, D., & Wang, C.: Cyclic Permeability Evolution During Repose Then Reactivation of Fractures and Faults, *Journal of Geophysical Research: Solid Earth*, **124**, (2019), 4492–4506.

Karner, S. L., & Marone, C.: Effects of loading rate and normal stress on stress drop and stick-slip recurrence interval, In J. Rundle, D. L. Turcotte, & W. Klein (Eds.), *Geocomplexity and the Physics of Earthquakes: Geophysical Monograph 120,* Amercian Geophysical Union, Washington D.C., (2000), 187–198.

Karner, S. L., & Marone, C.: Frictional restrengthening in simulated fault gouge: Effect of shear load perturbations, *Journal of Geophysical Research*, **106**, (2001), 19319–19337.

Karner, S. L., Marone, C., & Evans, B.: Laboratory study of fault healing and lithification in simulated fault gouge under hydrothermal conditions, *Tectonophysics*, **277**, (1997), 41–55.

Kilgore, B. D., Blanpied, M. L., & Dieterich, J. H.: Velocity dependent friction of granite over a wide range of conditions, *Geophysical Research Letters*, **20**, (1993), 903–906.

Kishida, K., Kawaguchi, Y., Nakashima, S., & Yasuhara, H.: Estimation of shear strength recovery and permeability of single rock fractures in shear-hold-shear type direct shear tests, *International Journal of Rock Mechanics and Mining Sciences*, **48**, (2011), 782–793.

Lockner, D. A., Summers, R., & Byerlee, J. D.: Effects of temperature and sliding rate on frictional strength of granite, *Pure and Applied Geophysics*, **124**, (1986), 445–469.

Lockner, D. A., Beeler, N. M., & Hickman, S. H.: Strength recovery and dependence on normal stress in hydrothermal quartzite tests, *Prodeedings,* 2019 AGU Fall Meeting, American Geophysical Union, San Francisco, CA, (2019).

Logan, J. M., & Rauenzahn, K. A.: Frictional dependence of gouge mixtures of quartz and montmorillonite on velocity, composition and fabric, *Tectonophysics*, **144**, (1987), 87–108.

Marone, C., & Scholz, C. H.: Particle-size distribution and microstructures within simulated fault gouge, *Journal of Structural Geology*, **11,** (1989), 799–814.

Mitchell, E. K., Fialko, Y., & Brown, K. M.: Temperature dependence of frictional healing of Westerly granite: Experimental observations and numerical simulations, *Geochemistry, Geophysics, Geosystems*, **14**, (2013), 567–582.

Moore, D. E., & Lockner, D. A.: Frictional strengths of talc-serpentine and talc-quartz mixtures, *Journal of Geophysical Research: Solid Earth*, **116**, (2011), 1–17.

Moore, D. E., Lockner, D. A., & Byerlee, J. D.: Reduction of permeability in granite at elevated temperatures, *Science*, **265,** (1994), 1558–1561.

Morrow, C. A., Moore, D. E., & Lockner, D. A.: Permeability reduction in granite under hydrothermal conditions, *Journal of Geophysical Research*, **106**, (2001), 30551-30560.

Nakatani, M. (1998). A new mechanism of slip weakening and strength recovery of friction associated with the mechanical consolidation of gouge. *Journal of Geophysical Research: Solid Earth*, *103*(B11), 27239–27256. https://doi.org/10.1029/98jb02639

Nakatani, M., & Mochizuki, H.: Effects of shear stress applied to surfaces in stationary contact on rock friction, *Geophysical Research Letters*, **23**, (1996), 869–872.

Nakatani, M., & Scholz, C. H.: Frictional healing of quartz gouge under hydrothermal conditions: 1. Experimental evidence for solution transfer healing mechanism, *Journal of Geophysical Research: Solid Earth*, **109**, (2004).

Olsen, M. P., Scholz, C. H., & Léger, A.: Healing and sealing of a simulated fault gouge under hydrothermal conditions: Implications for fault healing. *Journal of Geophysical Research*, **103***,* (1998), 7421-7430.

Peters, C. A.: Accessibilities of reactive minerals in consolidated sedimentary rock: An imaging study of three sandstones, *Chemical Geology*, **265**, (2009), 198–208.

Plummer, M., Bradford, J., Moore, J., & Podgorney, R.: *Reservoir response to thermal and high- pressure well stimulation efforts at Raft River, Idaho,* Idaho National Lab, Idaho Falls, ID, (2016).

Polak, A., Elsworth, D., Yasuhara, H., Grader, A. S., & Halleck, P. M.: Permeability reduction of a natural fracture under net dissolution by hydrothermal fluids, *Geophysical Research Letters*, **30**, (2003).

Rutter, E. H., & Mecklenburgh, J.: Hydraulic conductivity of bedding-parallel cracks in shale as a function of shear and normal stress, *Geological Society Special Publication*, **454**, (2017), 67–84.

Rutter, E. H., & Mecklenburgh, J.: Influence of Normal and Shear Stress on the Hydraulic Transmissivity of Thin Cracks in a Tight Quartz Sandstone, a Granite, and a Shale, *Journal of Geophysical Research: Solid Earth*, **123***,* (2018), 1262–1285.

Ryan, K. L., Rivière, J., & Marone, C.: The Role of Shear Stress in Fault Healing and Frictional Aging, *Journal of Geophysical Research: Solid Earth*, **123***,* (2018), 10,479-10,495.

Scott, D. R., Lockner, D. A., Byerlee, J. D., & Sammis, C. G.: Triaxial testing of Lopez Fault gouge at 150 MPa mean effective stress, *Pure and Applied Geophysics*, **142***,* (1994), 749–775.

Tembe, S., Lockner, D. A., & Wong, T. F.: Effect of clay content and mineralogy on frictional sliding behavior of simulated gouges: Binary and ternary mixtures of quartz, illite, and montmorillonite, *Journal of Geophysical Research: Solid Earth*, **115***,* (2010), 1–22.

Tenthorey, E., Cox, S. F., & Todd, H. F.: Evolution of strength recovery and permeability during fluid-rock reaction in experimental fault zones, *Earth and Planetary Science Letters*, **206***,* (2003), 161–172.

Tesei, T., Collettini, C., Carpenter, B. M., Viti, C., & Marone, C.: Frictional strength and healing behavior of phyllosilicate-rich faults, *Journal of Geophysical Research: Solid Earth*, **117***,* (2012), 1–13.

Yasuhara, H., Polak, A., Mitani, Y., Grader, A., Halleck, P., & Elsworth, D. (2006). Evolution of fracture permeability through fluid–rock reaction under hydrothermal conditions. *Earth and Planetary Science Letters*, *244*(1–2), 186–200.

Ye, Z., Janis, M., & Ghassemi, A.: Laboratory investigation of permeability evolution in shear stimulation of granite fractures for EGS, *Transactions - Geothermal Resources Council*, **41**, (2017) 985–1004.

Zimmerman, R. W., & Bodvarsson, G. S.: Hydraulic conductivity of rock fractures, *Transport in Porous Media*, **23***,* (1996), 1–30.